Journal of Digital Imaging (2018) 31:543–552
https://doi.org/10.1007/s10278-017-0048-5

Application of Color Transformation Techniques in Pediatric Spinal Cord MR Images: Typically Developing and Spinal Cord Injury Population

Mahdi Alizadeh[1,2] · Pallav Shah[3] · Chris J. Conklin[2] · Devon M. Middleton[2] · Sona Saksena[2] · Adam E. Flanders[2] · Laura Krisa[4] · MJ Mulcahey[4] · Scott H. Faro[4,5] · Feroze B. Mohamed[2]

Published online: 16 January 2018
© Society for Imaging Informatics in Medicine 2018

Abstract
The purpose of this study was to evaluate an improved and reliable visualization method for pediatric spinal cord MR images in healthy subjects and patients with spinal cord injury (SCI). A total of 15 pediatric volunteers (10 healthy subjects and 5 subjects with cervical SCI) with a mean age of 11.41 years (range 8–16 years) were recruited and scanned using a 3.0T Siemens Verio MR scanner. T2-weighted axial images were acquired covering entire cervical spinal cord level C1 to C7. These gray-scale images were then converted to color images by using five different techniques including hue-saturation-value (HSV), rainbow, red-green-blue (RGB), and two enhanced RGB techniques using automated contrast stretching and intensity inhomogeneity correction. Performance of these techniques was scored visually by two neuroradiologists within three selected cervical spinal cord intervertebral disk levels (C2-C3, C4-C5, and C6-C7) and quantified using signal to noise ratio (SNR) and contrast to noise ratio (CNR). Qualitative and quantitative evaluation of the color images shows consistent improvement across all the healthy and SCI subjects over conventional gray-scale T2-weighted gradient echo (GRE) images. Inter-observer reliability test showed moderate to strong intra-class correlation (ICC) coefficients in the proposed techniques (ICC > 0.73). The results suggest that the color images could be used for quantification and enhanced visualization of the spinal cord structures in addition to the conventional gray-scale images. This would immensely help towards improved delineation of the gray/white and CSF structures and further aid towards accurate manual or automatic drawings of region of interests (ROIs).

Keywords Pseudo-color transformation · Spinal cord injury · Gradient echo · Image enhancement

Introduction

There are 17,000 new spinal cord injury (SCI) cases each year in the USA according to a 2016 report by the National Spinal Cord Injury Statistical Center (NSCISC), and the total number of people who have SCI and are still alive is estimated to be 282,000 persons, with a range from 243,000 to 347,000 persons [1, 2]. There are various imaging methods to diagnose SCI. The initial test is generally a CT scan which can identify primarily bony pathology farther evaluations with MRI. MRI is excellent for evaluating soft tissues including the ligaments, intervertebral disks, nerves, and the spinal cord [2]. Unfortunately, MRI images of pediatric spinal cord are technically limited by various factors.

The main factor which degrades the quality of MR images can be classified under the broad category of physiological noise. Physiological noise is related to (1) the unique anatomic feature of the spinal cord. In particular, the small cross section area, large rostrocaudal extent, and curvature of the spinal cord which cause heterogeneity of signal within spinal cord because of partial volume effect, (2) the proximity of the

✉ Mahdi Alizadeh
mahdi.alizadeh.2@jefferson.edu

[1] Department of Neurosurgery, Thomas Jefferson University, 909 Walnut Street, Philadelphia, PA 19107, USA

[2] Jefferson Integrated Magnetic Resonance Imaging Center, Department of Radiology, Thomas Jefferson University, Philadelphia, PA, USA

[3] Department of Radiology, Temple University, Philadelphia, PA, USA

[4] Department of Occupational Therapy, Thomas Jefferson University, Philadelphia, PA, USA

[5] Department of Radiology, Johns Hopkins University, Baltimore, MD, USA

spinal cord to the several structures (vertebrae and intervertebral disks) increases variation in magnetic susceptibility and determines poor local magnetic field homogeneity causing image distortion and low signal intensity and (3) the physiological motion displaces the cord and generates signal intensity changes [4]. These movements are primarily due to the cardiac-driven pulsation of CSF within the subarachnoid space surrounding the cord. Another potential source of cardiac-related noise is the systole-induced pulsation in spinal arteries. It has been shown that cardiac noise is distributed irregularly along the full rostrocaudal extent. In addition, respiratory effects may either take the form of bulk movements of spinal and connective tissue, due to shifting tissue mass as the chest wall rises/falls, or to bulk changing susceptibility effects. This problem was previously noted in the brain, but it is of much greater significance to imaging of both the spinal cord and the brainstem [2–4].

The small cord volume requires higher resolution imaging which can be achieved, but requires additional scan time. Without extending scan time, standard imaging will result in low signal to noise ratio (SNR), and resolution [3]. Increasing the number of excitations will improve the SNR; however, it will also significantly increase scan time which is not desirable in pediatric imaging [3]. These issues present significant challenges to achieving a highly accurate and reproducible MRI signal to construct an image without distortion [5]. For many years, studies have proposed various acquisition methods and modifications to produce distortion-free images [6, 7]. However, some of the aforementioned artifacts remain and their impact may be reduced from additional post-processing methods such as image enhancement.

The human eye is more sensitive to a color image than a gray-scale image and has a superior memory for colors enabling wider dynamic range for color image than gray scale [6, 7]. Color transformation may offer improved visualization over gray-scale images and could improve MR diagnostics of the spinal cord. This may also aid the physicians to evaluate MRI exams faster. While color images are widely used in nonmedical image analysis applications, medical image analysis has traditionally relied on gray-scale images and less explored on color space due to physician preference and lack of standardization [8, 9]. Gray-scale presentation of MR images may reduce the contrast between small structures within the spinal cord, and this restriction is in part a result of the inadequacy of gray scale displays to capitalize on the full range of human visual perception [7]. The purpose of this study was to evaluate use of color transformation models for better differentiation of white and gray matter in the spinal cord and see if color transformation improves capability of the observer, board certified neuroradiologists, to detect the injured spinal cord in pediatric population.

In this research study, various widely used color transformation techniques such as red-green-blue (RGB), rainbow, and hue-saturation-value (HSV) were applied to the T2-weighted gradient echo (GRE) images obtained during standard clinical pediatric spinal cord imaging. RGB technique incorporated with two different enhancement options using automated contrast stretching and intensity inhomogeneity correction was also applied to these scans. Spinal cord images from healthy and SCI patients were processed to create color images using these five methods and compared with the conventional gray-scale GRE images. To the best of our knowledge, this has not been performed before for this medical imaging application.

Materials and Methods

Subjects

A total of 15 pediatric volunteers with a mean age of 11.41 years (range 8–16 years) were recruited. Subjects were divided into two groups including 10 healthy subjects who had no evidence of spinal cord injury (SCI) or pathology and 5 subjects with cervical spinal cord injury. Subjects and parents provided written information assent and consent of the institutional review board approved protocol. The inclusion criteria used for recruitment of the spinal cord injury group were as follows: subjects had stable cervical-level spinal cord injury as evidenced by no neurological change in the past 3 months and were at least 6-month post-cervical spinal cord injury. All patients were clinically assessed using the motor and sensory examinations of the International Standards for Neurological Classification of Spinal Cord Injury (ISNCSCI); severity of injury was determined according the American Spinal Injury Association Impairment Scale (AIS) [10]. Of the subjects with cervical SCI (Table 1), there were two patients classified as AIS A (complete spinal cord injury) and three with AIS D (sensory and motor incomplete).

Imaging

The MRI scans were performed using a 3.0T Siemens Verio MR scanner (Siemens Healthcare, Erlanger, Germany) with 4-channel neck matrix and 8-channel spine matrix coils. Manual shimming techniques were implemented to remove field inhomogeneities using linear shim coils. The protocol consists of a conventional sagittal turbo spin echo (TSE), T1-weighted scan, a sagittal TSE-T2-weighted scan, and an axial T2-weighted GRE. T2-weighted GRE images typically show good contrast between white and gray matter structures in the cervical spinal cord and adjacent normal appearing tissues [11].

Table 1 Demographic and clinical characteristics of the SCI patients

Subject	Age at the time of study	Age at the time of SCI	Level of injury based ISNCSCI	Severity of injury based AIS	MRI findings
SCI1	11.1	4.9	C6	A	Marked focal atrophy w/large focal syringomyelia (mid C7 to mid T1); Increased intramedullary signal w/mild atrophy (mid C6 to mid C7); no hemorrhage.
SCI2	8.1	3.8	C1	D	Subtle increase in intramedullary signal (C1); increased signal of left cord (C7–T1); no atrophy; no hemorrhage.
SCI3	13.8	0.5	C5	D	Mild atrophy (C6-C7 to C7-T1); no abnormal intramedullary signal; no hemorrhage.
SCI4	8.1	2.1	C8	A	Tiny focus of increased intramedullary signal (C6-C7); focal atrophy (mid C6 to C7-T1) marked at C6–C7 level; no hemorrhage
SCI5	12.4	1.5	C1	D	No abnormal intramedullary signal (C3-C7); no atrophy; no hemorrhage.

The imaging parameters included the following: voxel size = 0.42 × 0.42 × 6.0 mm^3, matrix size = 384 × 384, TR = 878 ms, TE = 7.8 ms, slice thickness = 6 mm, flip angle = 25°, number of averages = 1, and acquisition time = 156 s. Cardiac gating and respiratory compensation were not used in this study which increase acquisition time. Also, anesthesia was not administrated to the subjects in this study.

Psuedocolor Models

All the axial T2W-GRE images obtained from the healthy subjects and patients were post-processed using the various visualization improvement methods, which includes RGB, enhanced RGB models (RGB1 and RGB2), HSV, and rainbow as illustrated in Fig. 1. A pseudo-color images were derived from the gray-scale image by mapping each pixel value to a color according to a look up table or function [6, 12]. Color mapping is done overall with all the slices together to still preserve the same color which is assigned for the given anatomy throughout all the slices and between different patients.

In the RGB method, color changes smoothly from blue to red and passes through cyan, yellow, and orange [12]. Color components can be produced as below:

$$G = \begin{cases} 0 & I \le \Delta - 1 \\ \dfrac{I + 1 - \Delta}{n} & \Delta - 1 < I \le \Delta + n - 1 \\ 1 & \Delta + n - 1 < I \le \Delta + 2n - 2 \\ \dfrac{\Delta + 3n - I - 1}{n} & \Delta + 2n - 2 < I \le \Delta + 3n - 2 \end{cases} \quad (1)$$

where G represents component of the green channel in a color image, I represents the intensity value, $n = f(m/4)$ and $\Delta = f(n/2) - (mod(m/4) == 1)$, m is the number of color scales, and $f(x)$ rounds x to the nearest integer. The red and blue components can be obtained by shifting the green component to the right and left by the step of $n/(max(gray\ level))$, respectively [6].

In the rainbow transformation, the color is a variant of sine/cosine function. The rainbow color map uses as a default in many visualization systems, but the highly heterogeneous structures in the image can be hidden because of the lack of monotonic perceptual ordering [6, 13]. The color channels (i.e., R, G, and B) in an image can be obtained as follows:

$$R = \left(1 + \cos\left(\frac{4\pi}{3 \times 255} I\right)/2\right) \quad (2)$$

$$G = \left(1 + \cos\left(\frac{4\pi}{3 \times 255} I - \frac{2\pi}{3}\right)/2\right) \quad (3)$$

$$B = \left(1 + \cos\left(\frac{4\pi}{3 \times 255} I - \frac{4\pi}{3}\right)/2\right) \quad (4)$$

where I is the intensity level of each pixel in the monochromic image [6, 13].

HSV model, unlike RGB, separates luminance or image intensity, from chromatic or the color information. In HSV color space, hue, saturation, and value (or intensity) are the coordinate axis. Hue (H) component describes pure color and is in the form of angle between 0 and 360. Saturation (S) component gives measure of dilution of color with white color. The range of saturation is between 0 and 1, and finally, value or intensity (V) of the color corresponds to the brightness or gray level of the image. The range of value is between

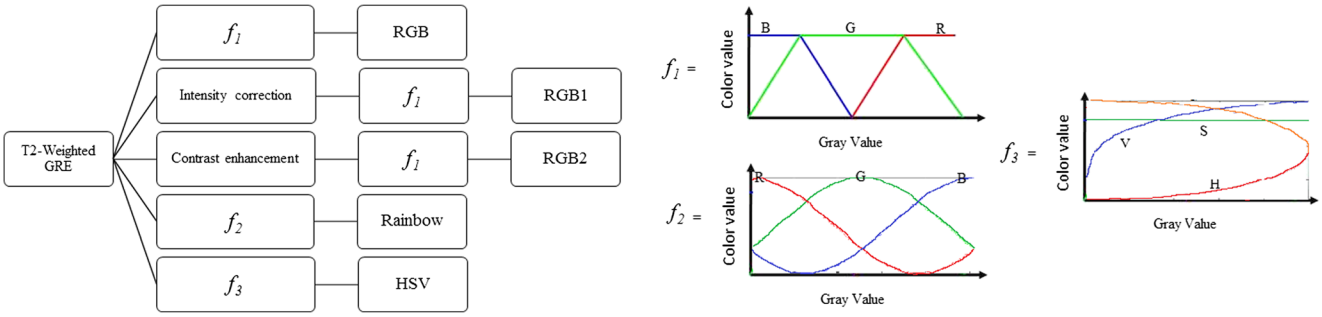

Fig. 1 Flowchart shows the creation of the pseudo-color maps that included RGB, RGB1, RGB2, rainbow, and HSV using different functions. Spectra for generating color components in RGB, rainbow, and HSV models have been shown by f_1, f_2, and f_3 functions, respectively. RGB1 and RGB2 models use same spectrum as RGB model (i.e., f_1 function) after performing intensity correction and contrast enhancement on gray-scale image

0 and 1 where 0 means black and 1 means white [14, 15]. H, S, and V components were generated from RGB color space as described below:

$$H = \begin{cases} \delta & if\ B \le G \\ 360 - \delta & if\ B > G \end{cases} \tag{5}$$

$$\delta = \arccos\left(\frac{(R-G)+(R-B)}{2\sqrt{(R-G)^2+(R-B)(G-B)}}\right) \tag{6}$$

$$S = 1 - 3 \times \frac{\min(R,G,B)}{R+G+B} \tag{7}$$

$$V = \frac{R+G+B}{3} \tag{8}$$

Two intensity correction methods including intensity inhomogeneity correction and automated contrast stretching were incorporated with RGB technique and named as RGB1 and RGB2, respectively, to improve the efficacy of color images [16, 17]. In the RGB1 color code, a nonlinear intensity compensation technique which uses only the pixel values instead of the homogeneous regions was performed as intensity inhomogeneity correction as follows:

$$g(u) = 255(u/255)^{\frac{1}{2+p\cos(\alpha(u))}},\quad \alpha(u) = \pi u/2x_m \tag{9}$$

where $p \in [0,1]$ is the weighting factor, P denotes the pixel interval (0,255), x denotes the pixel value, and x_m is the middle point of P [16–18].

In RGB2 model, the gray-scale image was enhanced first by stretching the range of intensity values. The enhancement model computed as follows:

$$s = (x-c)\left(\frac{\max(x)-\min(x)}{d-c}\right) + \min(x) \tag{10}$$

where x is the unmodified image, c and d are the lower and upper limits based on the histogram of the image. It is optimal to select c and d to be at 5 and 95% of the histogram of the original image [19, 20].

Data Analysis

The performance of the proposed techniques (see Fig. 1) was assessed by using visual inspection of GRE images and quantitative analysis. The quantitative analysis consists of a region of interest (ROIs) analysis of gray matter (GM) and white matter (WM) values and the contrast to noise ratio (CNR) between the GM and WM ROIs.

Quantitative Analysis

CNR and SNR SNR and CNR in GRE image and all five different color images were measured as described in

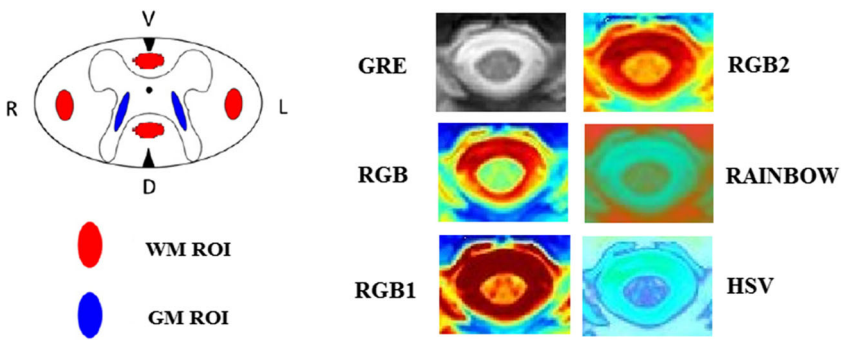

Fig. 2 The GM and WM ROIs depicted in the schematic drawing of the cross section of the spinal cord (GM and WM ROIs were highlighted in blue and red, respectively). The WM ROI covers parts of the left (L) and right (R) lateral funiculus as well as dorsal (D) and ventral (V) columns. The GM ROI covers parts of the central butterfly-shaped GM structure

Table 2 Criteria and scores for the visual evaluation of corrected images

Type of evaluation	Criteria	Score
Normality and abnormality of cord	Normal cord	1
	Abnormal cord	0
	Not defined	0
Accuracy	Completely obscuring the finding or pathology	0
	Significantly obscuring the finding or pathology	1
	Minimally improving the finding or pathology	2
	Significantly improving the finding or pathology	3
	Completely improving the finding or pathology	4
Differentiating gray and white matter	Completely obscuring the contrast between the gray and white matter	0
	Significantly obscuring contrast between the gray and white matter	1
	Minimally improving contrast between the gray and white matter	2
	Significantly improving contrast between the gray and white matter	3
	Completely improving contrast between the gray and white matter	4
Differentiating cord edge from CSF	Completely obscuring cord edge from CSF	0
	Significantly obscuring cord edge from CSF	1
	Minimally improving cord edge from CSF	2
	Significantly improving cord edge from CSF	3
	Completely improving cord edge from CSF	4
Homogeneity of CSF	Completely obscuring homogeneity of CSF	0
	Significantly obscuring homogeneity of CSF	1
	Minimally improving homogeneity of CSF	2
	Significantly improving homogeneity of CSF	3
	Completely improving homogeneity of CSF	4

eq. 3. Image noise was measured from a large area (approximately 500 mm^2) outside the object and defined as the standard deviation of background signal intensity (i.e., air). Eight ROIs were drawn to calculate SNR and CNR included two ROIs of GM (two samples in lateral sides), four ROIs of WM (ventral, dorsal, and lateral regions), one ROI of the whole cord, and one ROI of the air. The ROIs were chosen away from the border or edge of these tissues to avoid the effects of partial volume artifacts (Fig. 2). Note that SNR and CNR are unitless measures.

$$\begin{aligned} SNR &= \frac{mean_{cord}}{Standard\ Deviation_{Air}} \\ CNR &= \frac{mean_{WM} - mean_{GM}}{Standard\ Deviation_{Air}} \end{aligned} \tag{11}$$

Qualitative Analysis

Qualitative assessment entailed visual inspection of the spinal cord and structures within spinal canal on unimodal gray-scale image and five color images. All images individually were rated for overall quality of image named as accuracy (ACC), differentiating GM/WM structures (D(GM/WM)) and cord edge (CE) from CSF (D(CE/CSF)), and homogeneity of CSF (H(CSF)) using Likert type scale of 0–4 (4, excellent; 0, very poor) by two independent board certified neuroradiologists with a combined experience of 35 years (24 and 11 years). This scale included degradation due to motion artifacts, susceptibility artifacts, inhomogeneities artifacts, and SNR. The examiners were blinded to the type of data and methods. Also, the diagnostic performance of gray and color images in detecting normal or abnormal cords were examined in terms of sensitivity, specificity, and accuracy:

$$\begin{aligned} sensitivity &= \frac{TP}{TP + FN} \\ specificity &= \frac{TN}{TN + FP} \\ accuracy &= \frac{TP + TN}{TP + FP + TN + FN} \end{aligned} \tag{2}$$

where true positive (TP) is an abnormal cord which is correctly diagnosed as abnormal, false positive (FP) is a healthy cord which is incorrectly identified as unhealthy, true negative (TN) is a healthy cord correctly identified as healthy, and false negative (FN) is an unhealthy cord which is incorrectly identified as healthy. Table 2 describes the criteria used by examiners to evaluate color and unimodal gray-scale images.

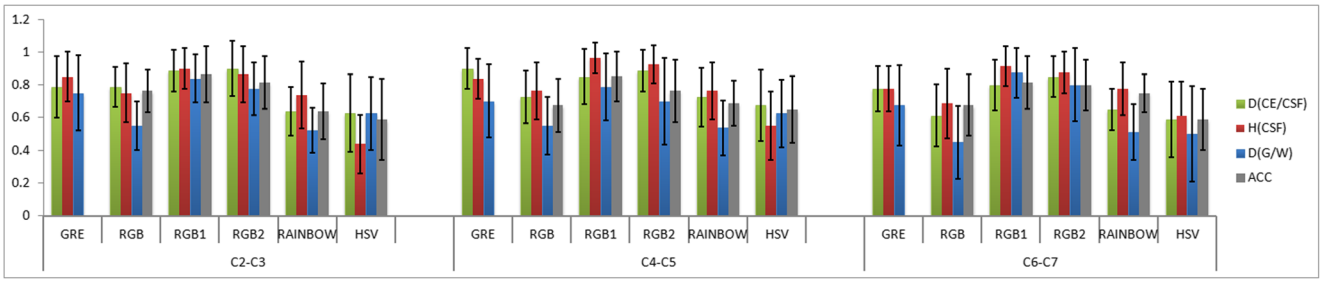

Fig. 3 Plot showing the visualization parameters including overall quality of image (ACC), differentiating GM/WM structures (D(GM/WM)), differentiating cord edge (CE) from CSF (D(CE/CSF)), and homogeneity of CSF (H(CSF)) as a function of cord level (upper (C2-C3), middle (C4-C5), and lower (C6-C7) cervical spinal cord levels) averaged across all the control subjects

Results

Qualitative and quantitative examination of pseudo-color transformation techniques showed reduction in motion-induced artifacts and well-defined CSF and cord structures.

Visual Inspection of GRE Images and Color Maps

Likert type scaling in the control subjects showed mean ± standard deviation GRE = 0.78 ± 0.17, RGB = 0.67 ± 0.17, RGB1 = 0.87 ± 0.17, RGB2 = 0.83 ± 0.17, rainbow = 0.66 ± 0.16, and HSV = 0.59 ± 0.22. The subjects with SCI showed reduced values compared with control subjects: GRE = 0.67 ± 0.21, RGB = 0.56 ± 0.19, RGB1 = 0.73 ± 0.23, RGB2 = 0.73 ± 0.22, rainbow = 0.56 ± 0.18, and HSV = 0.5 ± 0.31. The mean ± standard deviation of each visual inspection parameter, as a function of cord level, is illustrated in Figs. 3 and 4. In overall, there was a consistent increase in image quality compared to GRE images in RGB1 and RGB2 and decrease in RGB, rainbow, and HSV across all the healthy subjects. Statistically (using two-tailed t test) significant increase has been shown in RGB1 color map ($p = 0.04$), and significant decreases have been shown in RGB ($p = 0.02$), rainbow ($p < 0.001$), and HSV ($p < 0.001$) color maps. Observer rating in SCI group showed increases in RGB1 and RGB2 and decreases have been shown in RGB, rainbow, and HSV. However, no significant decrease/increase has been shown in these color maps across all SCI groups.

Reliability tests showed moderate to strong agreement between the two examiners. For the averaged visual inspection parameter values across selected levels, the ICCs and their 95% CIs were GRE [ICC = 0.73, CI (0.69–0.77)], RGB [ICC = 0.83, CI (0.58–0.65)], RGB1 [ICC = 0.85, CI (0.75–0.83)], RGB2 [ICC = 0.81, CI (0.74–0.82)], rainbow [ICC = 0.79, CI (0.58–0.66)], and HSV [ICC = 0.91, CI (0.49–0.6)].

Diagnostic Performance of Color Models

Figures 5 and 6 demonstrate how the different methods affected the diagnostic performance. The application of the proposed techniques (RGB1 and RGB2) on MRI data outperforms the gray-scale GRE data in sensitivity, specificity, and accuracy. The results reported in Tables 3 and 4 show that the performance of the proposed system is superior in performance terms including accuracy, specificity, and sensitivity when compared to the unimodal gray-scale images.

The percentage of abnormal region of the spinal cord which is correctly identified as abnormal (sensitivity) was

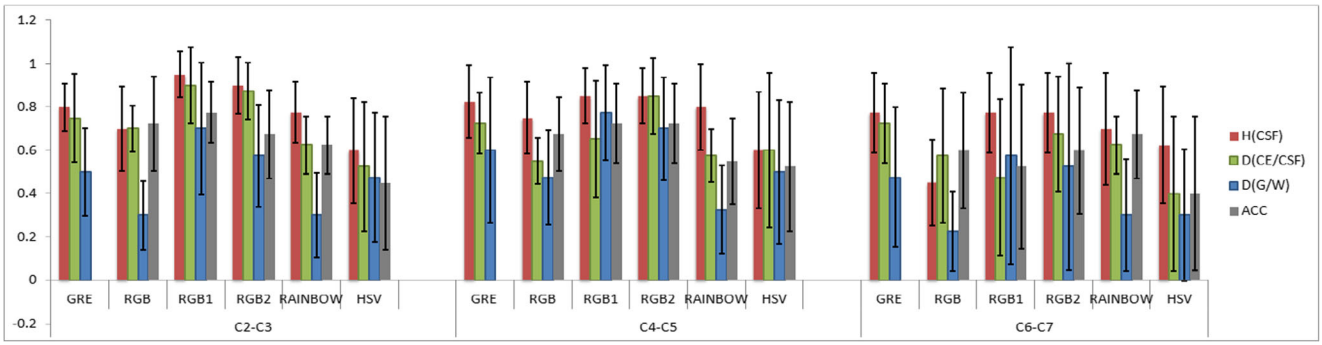

Fig. 4 Plot showing the visualization parameters including overall quality of image (ACC), differentiating GM/WM structures (D(GM/WM)), differentiating cord edge (CE) from CSF (D(CE/CSF)) and homogeneity of CSF (H(CSF)) as a function of cord level (upper (C2-C3), middle (C4-C5) and lower (C6-C7) cervical spinal cord levels) averaged across all the SCI subjects

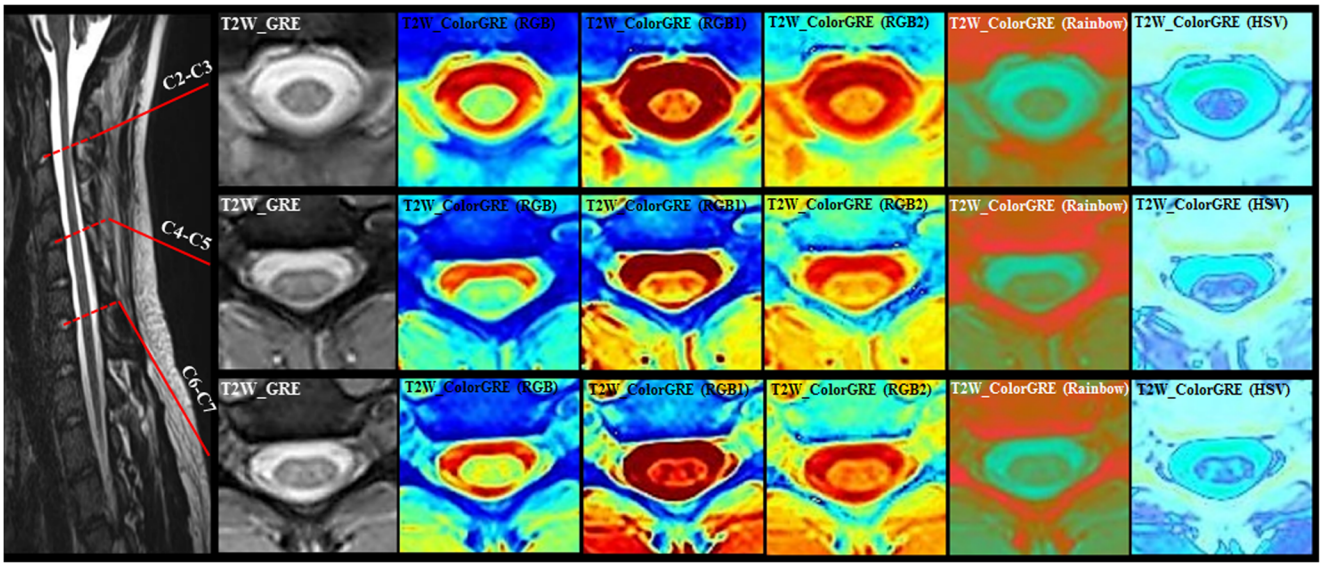

Fig. 5 T2W-GRE color maps at the three selected spinal cord levels (C2-C3, C4-C5, and C6-C7) for a heathy subject. Overall, the color images maximized the visualization of the CSF and structures within spinal cord such as GM and WM, the boundaries of GM from WM, cord edge from CSF, and CSF from surrounding tissues

increased by 5% using RGB1, RGB2, and HSV color maps. The percentage of normal regions of the spinal cord which are correctly identified as normal (specificity) increased by 13% using RGB1 and RGB2 and 10% using rainbow, and finally, the overall percentage of normal and abnormal cords which are correctly identified as normal and abnormal (accuracy) increased by 11% using RGB1 and RGB2 and 7% using rainbow. In the cases where color maps performed better than GRE with respect to specificity, the changes were due to healthy subjects being identified with confidence in the color images where they had been classified as "not defined" on GRE images.

Performance of Quantitative Assessments

The image quality of color GRE images as well as GRE images was evaluated using quantitative metrics of SNR and CNR as shown in Table 5. Also, the plot of SNR and CNR as a function of selected spinal cord levels are shown in Fig. 7.

Discussion

Poor tissue contrast, low SNR, and the small size of the spinal cord in MR cause challenges for interpretation of clinical

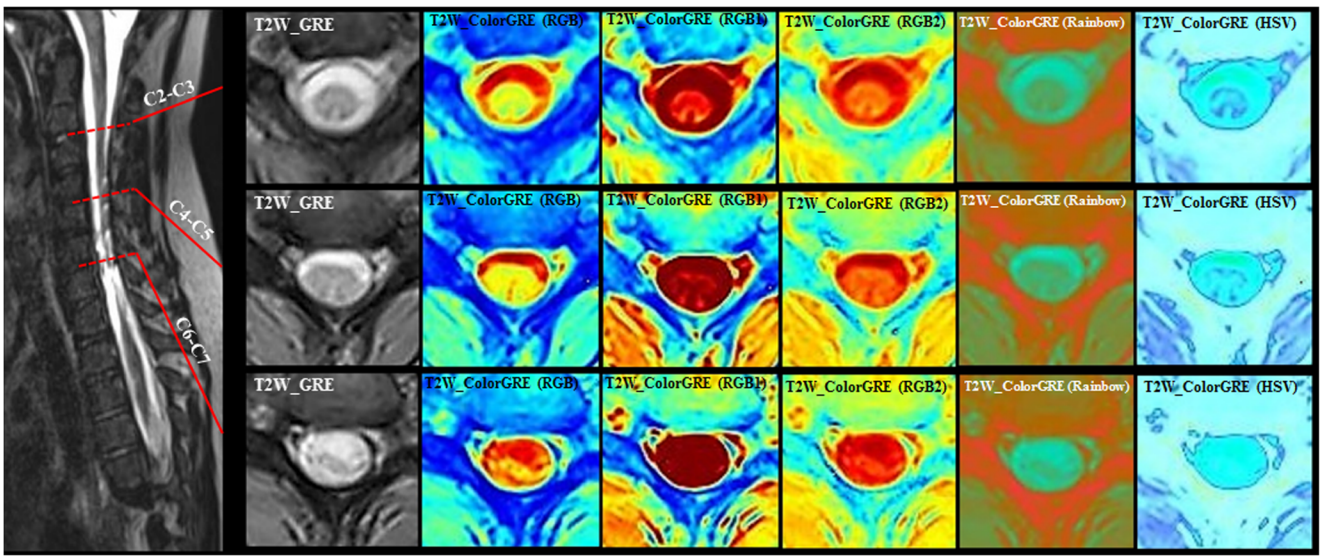

Fig. 6 T2W-GRE color maps at three different locations in the cervical cord for a SCI patient classified as AIS A (complete spinal cord injury). Level of injury-based ISNCSCI is at C8. MRI shows tiny focus of increased intramedullary signal (C6-C7); focal atrophy (mid C6 to C7–T1) at C6–C7 level

Table 3 Diagnostic performance measurements of gray-scale and proposed color images (%)

	GRE	RGB	RGB1	RGB2	RAINBOW	HSV
Sensitivity	75	65	80	80	70	80
Specificity	69	64	82	82	78	55
Accuracy	70	64	81	81	77	57

images [21–26]. The current study was undertaken to evaluate new methods for potentially enhancing the visualization of the T2-W GRE images by applying color imaging techniques that are widely used outside the medical imaging community. In this paper, some of the most successful of these techniques were developed and adopted to enhance the visualization of the spinal cord structures. While some efforts have been made in recent years to address various aspects of image enhancement for spinal cord MRI, this field is still poorly explored and reported in the literature [2, 3, 24].

The utilization of color maps has the potential to make spinal cord MR images more readily interpretable and more accurate for clinicians and researchers [7]. This approach potentially can provide qualitative improvements to currently used diagnostic MR images which can increase accuracy and confidence in visual assessment as well as improve quantitative measures. This could prove to be a powerful addition to characterize clinical spine pathologies such as SCI.

Table 4 The relevant confusion matrix of gray-scaled and color maps. Note that n is the number of gray-scaled images used for diagnostic evaluation by two certified neuroradiologists

$n = 90$	Predicted: NO	Predicted: YES	
Actual: NO	$TN_{GRE} = 48$	$FP_{GRE} = 22$	$\Sigma_{GRE} = 70$
	$TN_{RGB} = 48$	$FP_{RGB} = 27$	$\Sigma_{RGB} = 75$
	$TN_{RGB1} = 56$	$FP_{RGB1} = 13$	$\Sigma_{RGB1} = 69$
	$TN_{RGB2} = 56$	$FP_{RGB2} = 13$	$\Sigma_{RGB2} = 69$
	$TN_{RAINBOW} = 56$	$FP_{RAINBOW} = 16$	$\Sigma_{RAINBOW} = 72$
	$TN_{HSV} = 44$	$FP_{HSV} = 36$	$\Sigma_{HSV} = 80$
Actual: YES	$FN_{GRE} = 5$	$TP_{GRE} = 15$	$\Sigma_{GRE} = 20$
	$FN_{RGB} = 5$	$TP_{RGB} = 10$	$\Sigma_{RGB} = 15$
	$FN_{RGB1} = 4$	$TP_{RGB1} = 17$	$\Sigma_{RGB1} = 21$
	$FN_{RGB2} = 4$	$TP_{RGB2} = 17$	$\Sigma_{RGB2} = 21$
	$FN_{RAINBOW} = 5$	$TP_{RAINBOW} = 13$	$\Sigma_{RAINBOW} = 10$
	$FN_{HSV} = 3$	$TP_{HSV} = 7$	$\Sigma_{HSV} = 10$
	$\Sigma_{GRE} = 53$	$\Sigma_{GRE} = 37$	
	$\Sigma_{RGB} = 53$	$\Sigma_{RGB} = 37$	
	$\Sigma_{RGB1} = 60$	$\Sigma_{RGB1} = 30$	
	$\Sigma_{RGB2} = 60$	$\Sigma_{RGB2} = 30$	
	$\Sigma_{RAINBOW} = 61$	$\Sigma_{RAINBOW} = 29$	
	$\Sigma_{HSV} = 47$	$\Sigma_{HSV} = 43$	

Qualitative assessments were undertaken using gray-scale and color GRE images. The color images maximized the visualization of the CSF and structures within spinal cord such as GM and WM. Also, augment of the boundaries of GM from WM, cord edge from CSF, and CSF from surrounding tissues were particularly improved. Color visualization improved the delineation of these structural boundaries in comparison to conventional unimodal gray-scale images. These color maps reduce the abrupt variation in local pixel values by smoothing the input image (reducing the noise of an image) while decrease the CNR in an image. RGB1 color map uses sharpening function which is used to produce a crisper image with sharpening edges in order to highlight fine details (CNR increased up to 36%) while it increases the noise of an image.

Color transformation may aid in the visual inspection and analysis of images. This is primarily due to perception of the colors versus the gray scale. While the amount of information the human eye can perceive may change by transformation to color from gray scale but the absolute information content should not change because of the transform [6, 7], therefore, the SNR and CNR should not be different when the data is presented as gray scale or color. However, these values (SNR and CNR) will change when the image is transformed non-linearly as demonstrated in this work. In this case, the transformation changes the information content so that it differs from the measured data. Hence, the analysis is no longer performed on actual data. Non-linear transformation of the data will affect CNR and SNR, but actual improvement in data/image quality needs to support visually as well.

Reliability values for gray-scale and color images of the spinal cord were then estimated and compared using the ICC and showed moderate to strong agreement between the examiners (0.73–0.91). This provides a quantitative assessment of the efficacy of the color images for enhancing visualization and reliability. Inter-rater reliability estimates that color image tracings were considerably improved beyond those obtained using a gray-scale image.

The signal intensity drop-offs in the lower cervical levels (C4-C7) may be caused by cardiac-related artifacts (Fig. 7) and possibly coil non-uniformity at the edges of the coil. It increases the variability of qualitative and quantitative assessments. Cardiac gating might minimize the artifacts induced by cardiac movements and consequently decreases the variability however at the expense of increased acquisition time [25, 26].

Table 5 Quantitative assessments of averaged CNR between GM and WM and SNR in gray-scale and color T2- weighted GRE images

	GRE	RGB	RGB1	RGB2	RAINBOW	HSV
SNR	*76.92*	*130.6*	*50.58*	*110.69*	*82*	*97.29*
CNR	*45.1*	*14.76*	*61.35*	*38.27*	*4.84*	*22.51*

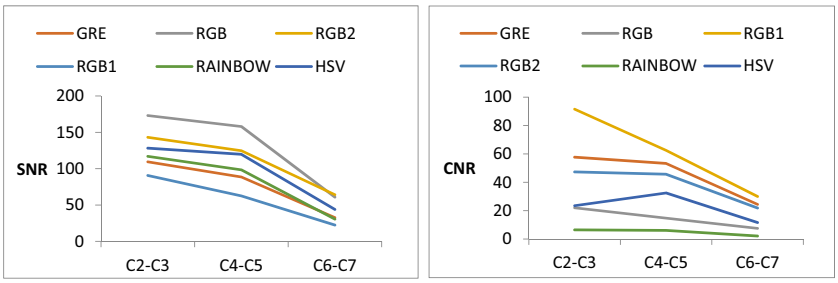

Fig. 7 Plots of SNR (left) and CNR (right) as a function of selected spinal cord levels for the GRE and color GRE images

Most diagnostic studies in the spinal cord were limited by the quality and resolution of MR images. Severity and localization of injury requires robust distinction between GM and WM. This study shows that the use of color transformation techniques can potentially improve the visual inspection of structures in the spinal cord and consequently incremental gains in the detection of pathologic states.

One of the limitation of this study is the relatively small sample size of the patient population ($n = 5$) as well as the type and location of the cervical injury. The small sample size limits the ability of the results to be adequately generalized over the entire pediatric SCI population. However, ICC and 95% CI values warrant that there is a real impact of color maps in improving the visualization. Additionally, the standard deviations for both healthy and patients are consistent between groups, which supports (though does not prove) the assumption of a reasonably good sample from each group. The results are encouraging and support the potential use of color images for better interpretation of gray-scale images and to improve our understanding of damage and recovery in diseased states of the spinal cord. Young children are more prone to high cervical injuries, with nearly 80% of injuries in children < 2 years old affecting this area. As the child approaches 8–10 years of age, the spinal anatomy and therefore injury pattern more closely approximate adult injuries [27]. Therefore, the proposed technique can easily apply on adult subject. In the future, we plan to increase the sample size and also look at the performance of this technique for the injuries in the lower spinal cord.

The computation time for the whole procedure applied on slab 1 which cover whole cervical and upper thoracic spinal cord (40 slices) was 75.1 ± 1.035 s/subject (mean ± SD) which includes reading, processing, and displaying the images. This was achieved using a standard Intel i5, 2.66 GHz processor with 3G of RAM and demonstrates its suitability in clinical practice.

Conclusion

The color mapping methods which are described in this paper have the possibility to be used in a wide range of medical imaging applications, such as monochrome image representation, enhancement, segmentation, and edge detection. In this study, visualization methods based on pseudo-color transformation are described to increase the conspicuity of spinal cord tissue in T2-W GRE axial images of the pediatric spinal cord. These new visualization methods demonstrate improvement in differentiating GM and WM within the spinal cord, differentiating cord edge from CSF and reduce the inhomogeneity caused by complex flow. Color images were noted to improve visualization and differentiation of normal from abnormal spinal cords in comparison to gray-scale images. One of the biggest challenges in evaluating spinal cord image analysis of SCI patients is confidently identifying the region of abnormality for ROI selection. Our results suggest that physicians can be more confident on drawing ROIs when they have both color and gray-scale images.

In overall, there was a consistent increase in image quality compared to GRE images in RGB1 and RGB2 using Likert type scaling as described in the manuscript (Figs. 3 and 4). Diagnostic performance shows that the percentage of abnormal region of the spinal cord which are correctly identified as abnormal (sensitivity) was increased by 5% using RGB1 and RGB2. The percentage of normal regions of the spinal cord which are correctly identified as normal (specificity) increased by 13% using RGB1 and RGB2, and finally, the overall percentage of normal and abnormal cords which are correctly identified as normal and abnormal (accuracy) increased by 11% using RGB1 and RGB2 (Table 3). Also, quantitative analysis shows that SNR and CNR were comparable in both RGB1 and RGB2 to the GRE images (Table 5).

Acknowledgments This work was supported by National Institute of Neurological Disorders of the National Institutes of Health under award number R01NS079635.

Compliance with Ethical Standards Subjects and parents provided written information assent and consent of the institutional review board approved protocol

References

1. Fisahn C, Aach M, Jansen O, Moisi M, Mayadev A, Pagarigan KT, Dettori JR, Schildhauer TA: The effectiveness and safety of exoskeletons as assistive and rehabilitation devices in the treatment of

neurologic gait disorders in patients with spinal cord injury: A systematic review. Global Spine Journal 6(8):822–841, 2016
2. Bickenback J: Launch of World Health Organization spinal cord injury report: International perspective on spinal cord injury. Geneva: WHO Press, 2013, 244p
3. Middleton DM, Mohamed FB, Barakat N et al.: An investigation of motion correction algorithms for pediatric spinal cord DTI in healthy subjects and Petients with spinal cord injury. Magnetic Resonance Imaging 32:433–439, 2014
4. Fratini M, Moraschi M, Maraviglia B, Giove F: On the impact of physiological noise in spinal cord functional MRI. J Magn Reson Imaging 40(4):770–777, 2014
5. Malisza KL, Martin T, Shiloff D et al.: Reactions of young children to the MRI scanner environment. Magn Reson Med 64:377–381, 2010
6. Koschan A, Abidi M: Digital color image processing, 1st edition. John and Sons Inc: Hoboken, New Jersey, 2008, 382p
7. Ward J, Magnotta V, Andreasen NC, Ooteman W, Nopoulos P, Pierson R: Color enhancement of multispectral MR images: Improving the visualization of subcortical structures. Journal of Computer Assisted Tomography 25(6):942–949, 2001
8. Siti Noraini Sulaiman, Nor Ashidi Mat Isa, Nor Hayati Othman, Nor Hayati Mohamed Noor. Pseudocolor Feature Extraction Technique for Cervical Cancer Pap Smear Image, IEEE 10th International Conference on ISDA, 2010; 314–319.
9. Tang H, Wu EX, Gallagher D, Heymsfield SB: Monochrome image representation and segmentation based on the Pseudocolor and PCT transformations, proceedings of the 23rd annual international conference of the IEEE in engineering in medicine and biology. Society 3:2696–2699, 2001
10. Krishblum SC: Et al. international standards for neurological classification of spinal cord injury: Case with classification challenges. The Journal of Spinal cord Medicine 37(2):120–127, 2014
11. Ozturk A, Aygun N, Smith SA, Caffo B, Calabresi PA, Reich DS: Axial 3D gradient Echo imaging for improved multiple sclerosis lesion detection in the cervical cord at 3T. Neuroradiology 55(4): 431–439, 2013
12. Suh PM, Jae-Yong B, Chang-Il C: Pseudocolor transformation for visualization of Ossicles in CT image. Acta oto-laryngologica 129: 515–520, 2009
13. David Borlan, Russel M. Taylor II. Rainbow Color Map (Still) Considered Harmful, IEEE Computer Society, 2007;14–17.
14. J. H. Jang and J. R. Ra. Pseudocolor image fusion based on intensity-hue-saturation color space, Proceeding of IEEE International Conference on Multisensor Fusion and Integration for Intelligent Systems, 2008; 366–371.
15. Govind B: Chavhan, Paul S. Babyn, Bejoy Thomas, Manohar M. Shroff, E. Mark Haacke. Principles, techniques and applications of T2*-based MR imaging and its applications. Radiographics 29(5): 1433–1449, 2009
16. Vovk U, Pernus F, Likar B: A review of methods for correction of intensity inhomogeneity in MRI. IEEE Transactions on Medical Imaging 26:405–421, 2007
17. Styner M, Brechbuhler C, Szekely G, Gerig G: Parametric estimate of intensity Inhomogeneities applied to MRI. IEEE Transcations on Medical Imaging 19:153–165, 2000
18. Mahdi Alizadeh, Feroze B. Mohamed, Scott H. Faro, Pallav Shah, Chris J. Conklin, Devon M. Middleton, Sona Saksena, Shiva Shahrampour, MJ Mulcahey. Intensity Inhomogeneity Correction in Clinical Pediatric Spinal Cord MRI Images, IEEE 41th Annual Northeast Bioengineering Conference (NBEC), 2015; 1–2.
19. Alizadeh M, Talebpour A, Soltanian-Zadeh H, Aghamiri S. M. R. Effects of Improved Adaptive Gamma Correction Method on Wireless Capsule Endoscopy Images: Illumination Compensation and Edge Detection, ICEE 2012; 1544–1548.
20. Alizadeh M, Soltanian Zadeh H, Haji Maghsoudi O. Segmentation of Small Bowel Tumors in Wireless Capsule Endoscopy Using Level Set Method, IEEE CBMS, 2014; 562–563.
21. Sharma DP: Intensity transformation using contrast limited adaptive histogram equalization. International Journal of Engineering Research:282–285, 2013
22. Muniyappan S, Allirani A, Saraswathi S. A Novel Approach for Image Enhancement by Using Contrast Limited Adaptive Histogram Equalization Method, 4th ICCNT, 2013;1–6.
23. Mohamed FB, Hunter LN, Barakat N, Liu C-SJ, Sair H, Samdani AF, Betz RR, Faro SH, Gaughan J, Mulcahey MJ: Diffusion tensor imaging of the pediatric spinal cord at 1.5T: Preliminary results. AJNR Am J Neuroradiol 32:339–345, 2011
24. Lin X, Tench CR, Turner B, Blumhardt LD, Constantinescu CS: Spinal cord atrophy and disability in multiple sclerosis over four years: Application of a reproducible automated technique in monitoring disease progression in a cohort of the interfere β-1α (Relif) treatment trial. J Neural Neurosurg Psychiatry 74:1090–1094, 2003
25. Chris J: Conklin, Devon M. Middleton, Mahdi Alizadeh and et al. spatially selective 2D RF inner field of view (iFOV) diffusion kurtosis imaging (DKI) of the pediatric spinal cord. NeuroImage: Clinical 11:61–67, 2016
26. Alizadeh M, Intintolo A, DM Middleton CJ, Conklin SH, Faro MJ, Mulcahey FB: Mohamed. Reduced FOV diffusion tensor MR imaging and fiber tractography of pediatric cervical spinal cord injury. Spinal Cord:1–7, 2016
27. Proctor MR: Spinal cord injury. Crit Care Med 30(11 Suppl):S489–S499, 2002